J Therm Anal Calorim (2009) 97:167–172
DOI 10.1007/s10973-009-0244-8

Influence of the thermal treatment in the crystallization of $NiWO_4$ and $ZnWO_4$

A. L. M. de Oliveira · J. M. Ferreira · Márcia R. S. Silva · Soraia C. de Souza · F. T. G. Vieira · E. Longo · A. G. Souza · Iêda M. G. Santos

ICTAC2008 Conference

Abstract $NiWO_4$ and $ZnWO_4$ were synthesized by the polymeric precursor method at low temperatures with zinc or nickel carbonate as secondary phase. The materials were characterized by thermal analysis (TG/DTA), infrared spectroscopy, UV–Vis spectroscopy and X-ray diffraction. $NiWO_4$ was crystalline after calcination at 350 °C/12 h while $ZnWO_4$ only crystallized after calcination at 400 °C for 2 h. Thermal decomposition of the powder precursor of $NiWO_4$ heat treated for 12 h had one exothermic transition, while the precursor heat treated for 24 h had one more step between 600 and 800 °C with a small mass gain. Powder precursor of $ZnWO_4$ presented three exothermic transitions, with peak temperatures and mass losses higher than $NiWO_4$ has indicating that nickel made carbon elimination easier.

Keywords Wolframite · $ZnWO_4$ · $NiWO_4$ · Thermal treatment · Order–disorder

A. L. M. de Oliveira (✉) · J. M. Ferreira · M. R. S. Silva · S. C. de Souza · F. T. G. Vieira · A. G. Souza · I. M. G. Santos
Depto de Química, Laboratório de Combustíveis e Materiais, UFPB, João Pessoa, PB, Brazil
e-mail: andrel_ltm@hotmail.com

J. M. Ferreira
COAMA, Centro Federal de Educação Tecnológica da Paraíba, CEFETPB, João Pessoa, PB, Brazil

E. Longo
CMDMC, Centro Multidisciplinar de Desenvolvimento de Materiais Cerâmicos, UNESP, Araraquara, SP, Brazil

Introduction

Transition metal tungstates are technologically important materials which have been attracting attention from researchers due to their interesting physical and chemical properties. For instance, they can be applied as scintillation detectors, laser hosts, photoanodes, optical fibers, microwave applications, humidity sensors, pigments, etc. [1, 2]. Among these tungstates, nickel tunsgate ($NiWO_4$) and zinc tungstate ($ZnWO_4$) have been extensively studied. $NiWO_4$ has important electrochromic properties, besides a high long-lasting structural stability [3] and good catalytic properties [2]. $ZnWO_4$ has some advantages over other materials, as high chemical stability, high average refractive index, high light yield, short decay time, and low afterglow to luminescence [4, 5].

These tungstates crystallize with wolframite structure that has monoclinic unit cell, space group P2/c or C_{2h}^4 characterized by alternating layers of transition metal and tungsten atoms parallel to the (100) plane [6].

Several methods of chemical synthesis have gained popularity for preparation of ceramic oxides, including tungstates. Among these methods, sol–gel, co-precipitation, hydrothermal, citrate gel, polymeric precursors and gel combustion can be cited [1, 7]. Chemical and physical properties of metal oxides including tungstates are generally dependent on synthesis route.

In this work, $NiWO_4$ and $ZnWO_4$ were obtained by the polymeric precursor method [8–10] that has been successfully used in the synthesis of nanoparticles and thin films of polycationic oxides, including tungstates [1]. The objective of this work was the evaluation of the organic material elimination and the wolframite short and long range ordering according to the lattice modifier—zinc or nickel.

Experimental

Nickel tungstate ($NiWO_4$) and zinc tungstate ($ZnWO_4$) were obtained by the polymeric precursor method, as previously described [1, 11, 12]. After synthesis of the powder precursors, they were milled in an attritor mill in alcoholic media for 4 h followed by calcination at 350 °C for 12 h in oxygen atmosphere for organic material elimination. The powder precursors were characterized using thermogravimetry (TG) and differential thermal analysis (DTA) (SDT 2980—TA Instruments) in air atmosphere with a flow rate of 110 mL min^{-1} and at a heating rate of 10 °C min^{-1} up to 900 °C. About 10 mg of sample were weighted into alumina pans. Characterization was also done by infrared spectroscopy (IR), X-ray diffraction (XRD) and UV–Vis spectroscopy. IR analyses were performed using an MB-102 Bomem spectrophotometer, in the range of 400–2000 cm^{-1}, using KBr pellets. XRD patterns were obtained using a D-5000 Siemens diffractometer employing Kα Cu radiation. The UV–Vis spectra were obtained in a spectrophotometer (UV-2550 Shimadzu) at the 190–900 nm wavelength range after calcination of $NiWO_4$ at 700 °C/2 h.

Results and discussion

The thermogravimetric curves of the powder precursors are presented in Fig. 1a and b. Comparing to literature data [10, 13], a meaningful decrease in mass loss was observed, indicating that the thermal treatment of the milled powder precursor was successful in the carbon elimination.

The thermal curves of the powder precursor of $NiWO_4$ heat treated for 12 h showed two mass loss steps (Fig. 1a and Table 1). The first one was endothermic, being assigned to the elimination of water and gases adsorbed on the powder surface. The second one was exothermic, being assigned to the combustion of the organic material. The powder precursor thermally treated for 24 h had one more step between 600 and 842 °C, with a small mass gain (Table 1).

In relation to the thermal decomposition of the powder precursors of $ZnWO_4$ (Fig. 1b and Table 1), a higher mass loss was observed, comparing to $NiWO_4$. When calcination was done at 12 h, the profile was similar to the $NiWO_4$ (12 h) one. When calcination was done for 24 h, four thermal decomposition steps were observed. The first one had an endothermic peak assigned to the elimination of water and gases adsorbed on the powder surface. The others had exothermic peaks, assigned to the combustion of the organic material. It was observed that a longer calcination time at 350 °C did not lead to a decrease in the amount of organic material. Moreover, this second calcination made carbon elimination more difficult, as indicated by the presence of one more step above 700 °C. This behavior may be assigned to the formation of intermediate

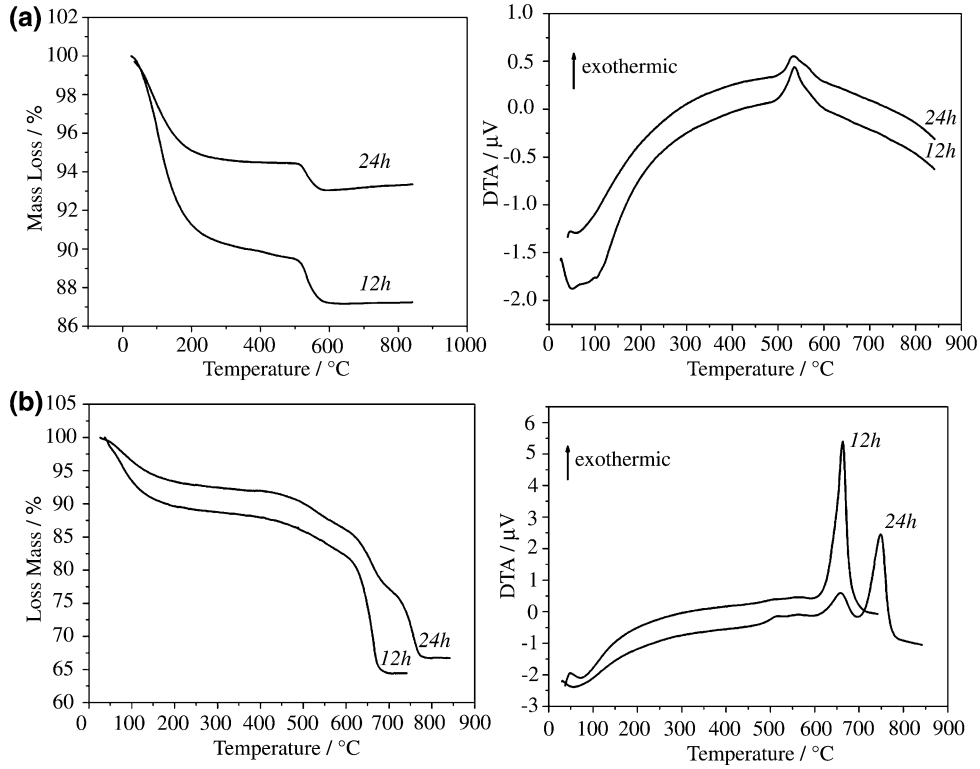

Fig. 1 Thermal analyses (TG/DTA) of the powder precursors of **a** $NiWO_4$ and **b** $ZnWO_4$ after partial carbon elimination

Table 1 Results of TG/DTA analyses for the powder precursors of $NiWO_4$ and $ZnWO_4$

Samples	Steps	Temperature range (°C)	Mass loss (%)	DTA peak temperature (°C)	DTG peak temperature (°C)
$NiWO_4$					
12 h	1	28–387	10.0	50.3 (endo)	101.5
	2	387–473	0.3	Not observed	423.8
	3	473–663	2.4	535.6 (exo)	533.2
24 h	1	42–487	4.5	58.2 (endo)	92.2
	2	487–600	1.2	533.3 (exo)	532.3
	3	632–842	+0.3	–	–
$ZnWO_4$					
12 h	1	38–280	11.1	71.8 (endo)	77.3
	2	280–710	24.5	663.3 (exo)	663.3
24 h	1	28–379	7.9	60.4 (endo)	75.5
	2	401–562	4.5	523.5 (exo)	515.8
	3	562–712	11.1	664.3 (exo)	659.6
	4	712–803	9.6	758.3 (exo)	756.3

compounds, which were already observed by other authors [14].

For $ZnWO_4$ (12 h), the onset temperature of the second step was 280 °C, which was lower than the calcination temperature (350 °C). When the precursor was thermally treated at this same temperature for 24 h, the onset temperature of the second step was 401 °C. This result was related to kinetic factors, showing that the precursor did not reach the equilibrium after 12 h of calcination at 350 °C.

Wang et al. [15] evaluated the thermal decomposition of nickel citrate intercalated into a layered double hydroxide using TG/DTA coupled to a mass spectrometer. The same steps observed in the present work were found—below 250 °C, only water was released, while the second step involved liberation of CO_2 and H_2O, characterizing a combustion reaction. For the nickel sodium citrate, the formation of carbonate was observed. Gajbhiye and Prasad [14] studied the thermal decomposition of hexahydrated nickel iron citrate and zinc iron citrate [16] in two different works. They observed that the first step was assigned to the citrate dehydration assigned to an endothermic peak. Exothermic combustion reactions led to the formation of an intermediate metastable compound with evolution of CO gas and to the formation of the respective oxides at higher temperatures.

Comparing the decomposition of the precursors of $NiWO_4$ and $ZnWO_4$, it was noticed that the peak temperatures were higher for $ZnWO_4$ with higher mass losses, indicating that zinc made carbon elimination more difficult. This behavior was also observed in literature for other systems containing zinc [8]. Unfortunately, we did not find literature data about pure nickel and zinc citrates decomposed at the same conditions. This way, literature data about the oxalate decomposition were used for comparison with the present results.

Dollimore et al. [17] evaluated the thermal decomposition of different oxalates in air and in N_2 atmosphere. It was observed that the decomposition temperature of zinc and nickel oxalates in air were 390 and 352 °C, respectively. In oxalates of bivalent metals, the extent to which the Me–O bond is covalent depends on the electronegativity of the metal. Decomposition will occur when a temperature is reached at which rupture of the M–O link is possible, or at which rupture of C–O bond occurs. The decomposition of NiC_2O_4 in nitrogen atmosphere gives Ni metal. In air, the metal formed in the decomposition is oxidized to metal oxide. For ZnC_2O_4 decomposition, ZnO is formed in air or in nitrogen atmosphere. For those oxalates which produce the metal in nitrogen the decomposition temperature represents the temperature at which the M–O link is ruptured and will depend critically on the size and charge of the metal ion, whereas in those decompositions where the oxide is produced in nitrogen the decomposition temperature represents the energy required to break the C–O bond and this will depend less critically on the nature of the cation.

Based on these results, we believe that the mass gain observed in the precursor of $NiWO_4$ (24 h) was due to the nickel oxidation, as TG/DTA analysis was done in air. This mass gain was not observed for $ZnWO_4$, as citrate decomposition probably led to ZnO formation.

UV–Vis spectra of $NiWO_4$ after calcination at 700 °C was used to evaluate the oxidation state of the cations (Fig. 2). According to Lo Jacono et al. [18], $Ni^{2+}O_6$ has absorption bands at 1.21, 1.65–1.74, 2.00–2.11, 2.83–2.88 and 3.35 eV due to the transition from $^3A_{2g}$ to the excited

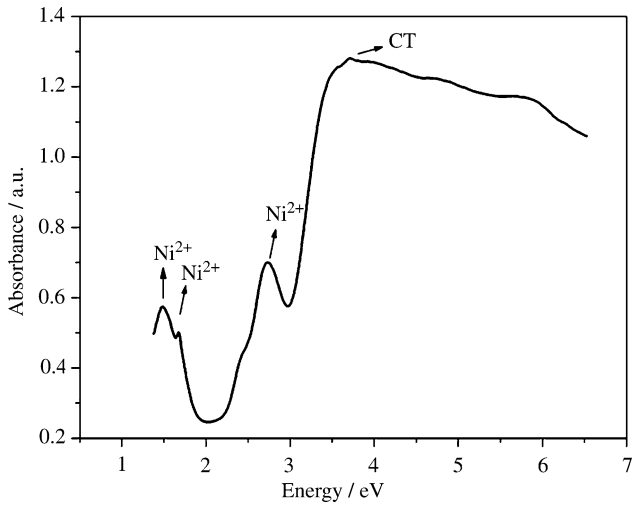

Fig. 2 UV–Vis spectra of the $NiWO_4$ after heat treatment at 350 °C for 12 and 24 h in oxygen atmosphere and calcination at 700 °C for 2 h. *CT* charge transfer

states $^3T_{2g}$, ^1E_g, $^3T_{1g}$, $^1T_{2g}$ and $^3T_{1g}$, respectively. This data is confirmed by Lenglet et al. [19] who reported the same bands at about 1.08–1.13, 1.72–1.75, 1.77–1.95, 2.71–2.79 and 2.97–3.00 eV. Llusar et al. [20] also reported spin-free ligand field absorption energies at 1.07, 1.66, 1.83, 2.67 and 3.04 eV for the same transitions reported above.

Another possibility for UV–Vis absorption bands was the presence of W^{5+}. Lin et al. [21] synthesized an organic–inorganic hybrid $(H_2en)(Hen)_2[H_2P_2W_5O_{23}]_5{\cdot}42H_2O$ by the hydrothermal method at 140 °C for 7 days, and observed an intervalence charge transfer transition (IVCT), $W^{6+} \rightarrow W^{5+}$, at 2.76 eV and a W^{5+} d–d transition at 2.95 eV. As the band at 2.95 eV was not observed in the present work, we believe that W^{5+} was not present after calcination at 700 °C.

In the present work, absorbance bands at 1.48, 1.67, 2.74 and 3.7 eV were observed, being the first two bands of low intensity localized in the blue range and the third and fourth ones of high intensity localized in the ultraviolet range. These bands were assigned to the presence of Ni^{2+} or to a charge transfer between clusters. Bands at 1.67 and 2.74 eV were assigned to the forbidden electronic transition from $^3A_{2g}$ to ^1E_g and $^1T_{2g}$, respectively. The last band at 3.7 eV may be related to charge transfer transitions. The band at 1.48 eV could not be assigned to $Ni^{2+}O_6$. Du Mont et al. [18] reported that $Ni^{2+}O_4$ presents a $^3T_1 \rightarrow {}^1T_2$ transition at 1.56–1.60 eV. Based on this information, we believe that the band at 1.48 eV is assigned to the presence of $Ni^{2+}O_4$ indicating that Frenkel defects are present in $NiWO_4$ with the dislocation of Ni^{2+} from octahedral to tetrahedral sites.

Figure 3 shows the IR spectra of the precursors of $NiWO_4$ and $ZnWO_4$ after thermal treatment at 350 °C for 12 and 24 h in oxygen atmosphere. Band assignments are presented in Table 2.

For wolframite, the total representation of the P2/c unit cell contains 18 Raman-active modes ($8A_g + 10B_g$), 15 infrared-active modes ($7A_u + 8B_u$), and 3 acoustic vibrational modes ($A_u + 2B_u$) [22, 23].

The wolframite structure is constituted by WO_6 polyhedra, with a dense packing of these coordination polyhedra in the unit cell. The tungstate ions are additionally connected to each other by means of intermolecular interactions of the $W^O{}_OW$ type. The characteristic vibrational bands corresponding to this structural fragment appear at the 500–700 and 220–280 cm^{-1} regions and are assigned to stretching and bending modes of the $W^O{}_OW$ unit, respectively [24, 25]. These bands are not observed for tungstates with scheelite structure, which have only WO_4 polyhedra.

Literature data about the scheelite structure points out the presence of WO_4–WO_3 at the beginning of the crystallization process. With temperature increase, the formation of WO_4 polyhedra is favored [26]. In the present work, a different behavior was observed for the precursors of $ZnWO_4$ and $NiWO_4$, in relation to the formation and bonding between WO_6 polyhedra, which determines the short-range ordering of the wolframite structure. While intense bands

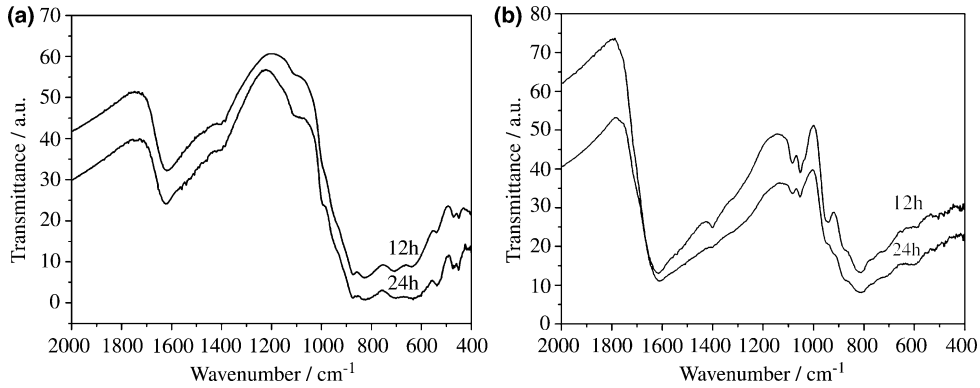

Fig. 3 IR spectra of $NiWO_4$ (**a**) and $ZnWO_4$ (**b**) after heat treatment at 12 and 24 h in oxygen atmosphere

Table 2 Assignment of the infrared spectra of the precursors of $NiWO_4$ and $ZnWO_4$ after thermal treatment at 350 °C for 12 and 24 h in oxygen atmosphere

$NiWO_4$ (cm^{-1})		$ZnWO_4$ (cm^{-1})		Assignment	Reference
12 h	24 h	12 h	24 h		
1619	1621	1617	1612	COO^- monodentate, $\nu(H_2O)_l$	[28]
1406_{sh}	1404_{sh}	1401	1401_{sh}	MeO_6 and $\nu(CO_3)^{2-}$	[28, 29]
1110	1104	1083, 1052	$1083, 1052_s$	MeO_6 and $\nu(CO_3)^{2-}$	[28, 29]
995_{sh}	991_{sh}	946	943_{sh}	$\nu_s(WO_6)^{6-}$	[25]
876_s	876_s	879_{sh}	876_{sh}	$\nu_{as}(WO_6)^{6-}$, $\nu(W^O{}_OW)$—st and $\nu(CO_3)^{2-}$	[25, 29]
826_b	826_b	814	812_{br}	$\nu_{as}(WO_6)^{6-}$ and $\nu(W^O{}_OW)$—st	[25]
710	704	722_{sh}	717_{sh}	$\nu_{as}(WO_6)^{6-}$ and $\nu(W^O{}_OW)$—st	[25]
639	635	595	595_{br}	$\nu_{as}(WO_6)^{6-}$ and $\nu(W^O{}_OW)$—st	[25]
539_s	539	–	–	$\nu_{as}(WO_6)^{6-}$ and $\nu(W^O{}_OW)$—st	[25]
$471, 450_s$	474, 452	–	–	$\delta_s(WO_6)^{6-}$—bd	[25]

Band characteristics: *s* small, *vs* very small, *sh* shoulder, *br* broad

Vibration modes: *st* stretching mode, *bd* bending mode, *l* lattice

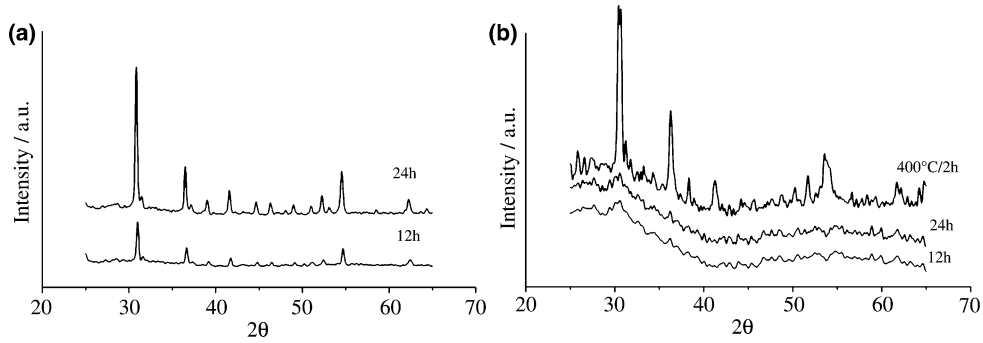

Fig. 4 XRD patterns of the **a** $NiWO_4$ and **b** $ZnWO_4$ after the thermal treatment at 350 °C for 12 and 24 h in oxygen atmosphere and also at 400 °C for 2 h, for $ZnWO_4$

were observed between 900 and 400 cm^{-1} for $NiWO_4$, only one broad band was observed at about 800 cm^{-1} for $ZnWO_4$, besides a low definition band around 600 cm^{-1} (Table 2). This result indicated that a higher short range order was observed for $NiWO_4$, which had the same bands observed by Hanuza et al. [25] and Frost et al. [27].

This behavior may be related to the organic material elimination, described by TG/DTA data, which is easier for the precursor of $NiWO_4$. This result was also observed in the IR spectra. Bands around 1610–1620 cm^{-1} were observed due to the presence of COO^- groups of ester monodentated complexes [1, 28, 29]. Bands assigned to carbonate groups were also observed at about 1400, 1080–1100 and 876 cm^{-1}. These bands were more intense in the precursor of $ZnWO_4$ than in $NiWO_4$ one.

As a consequence of the carbon elimination and short-range ordering of $NiWO_4$, a long-range ordering was already observed at this low calcination temperature, as showed in the XRD patterns (Fig. 4). The peaks observed were assigned to the wolframite structure with a monoclinic unit cell, identified by JCPDS card 72-0480 for $NiWO_4$ and 89-0447 for $ZnWO_4$. For $NiWO_4$, the intensities of the peaks increased meaningfully after calcination for 24 h. $ZnWO_4$ presented a completely different behavior, with a broad band characteristic of a disordered system, even after calcination for 24 h. Wolframite crystallization only occurred after one more calcination at 400 °C for 2 h.

Conclusions

The results obtained for $ZnWO_4$ and $NiWO_4$ synthesis by the polymeric precursor method showed different results, indicating that the lattice modifier determined the wolframite crystallization. For $ZnWO_4$ precursor, highly stable organic compounds were formed, being stable up to 700–800 °C. As a consequence, bonding among WO_6 octahedra got more difficult and the crystallization only occurred after calcination at 400 °C. For $NiWO_4$ precursor, organic compounds were easier to eliminate so that complete decomposition occurred below 600 °C. In this sample, infrared spectra showed that bonding among WO_6 octahedra was already observed after calcination at 350 °C, leading to a higher long-range order and well defined peaks in the XRD patterns.

References

1. de Oliveira ALM, Ferreira JM, Silva MRS, Braga GS, Soledade LEB, Maurera MAMA, et al. Yellow $Zn_xNi_{1-x}WO_4$ pigments obtained using a polymeric precursor method. Dyes Pigm. 2008;77:210–6.
2. Quintana-Melgoza JM, Cruz-Reyes J, Avalos-Borja M. Synthesis and characterization of $NiWO_4$ crystals. Mater Lett. 2001;47: 314–8.
3. Kuzmin A, Purans J. XAS, XRD, AFM and Raman studies of nickel tungstate electrochromic thin films. Electrochim Acta. 2001;46:2233–6.
4. Lou Z, Hao J, Cocivera M. Luminescence of $ZnWO_4$ and $CdWO_4$ thin films prepared by spray pyrolysis. J Lumin. 2002;99:349–54.
5. He HY. Luminescence properties of $NiWO_4$ powders and films prepared with novel methods. Mater Res Innov. 2008;12:138–41.
6. Ejima T, Banse T, Takatsuka H, Kondo Y, Ishino M, Kimura N, et al. Microscopic optical and photoelectron measurements of MWO_4 (M = Mn, Fe, and Ni). J Lumin. 2006;119:59–63.
7. Sen A, Pramanik P. A chemical synthetic route for the preparation of fine-grained metal tungstate powders (M = Ca, Co, Ni, Cu, Zn). J Eur Ceram Soc. 2001;21:745–50.
8. Gouveia DS, Soledade LEB, Paskocimas CA, Longo E, Souza AG, Santos IMG. Color and structural analysis of $Co_xZn_{7-x}Sb_2O_{12}$ pigments. Mater Res Bull. 2006;41:2049–56.
9. Xavier CS, Candeia RA, Bernardi MIB, Lima SJG, Longo E, Paskocimas CA, et al. Effect of the modifier ion on the properties of $MgFe_2O_4$ and $ZnFe_2O_4$ pigments. J Therm Anal Calorim. 2007;87:709–13.
10. Souza SC, Santos IMG, Silva MRS, Cássia-Santos MR, Soledade LEB, Souza AG. Influence of pH on iron doped Zn_2TiO_4 pigments. J Therm Anal Calorim. 2005;79:451–4.
11. Pôrto SL, Longo E, Pizani PS, Boschi TM, Simões LGP, Lima SJG, et al. Photoluminescence in the $Ca_xSr_{1-x}WO_4$ system at room temperature. J Solid State Chem. 2008;181:1876–81.
12. Pehini MP. US Patent No. 3330697, July (1967).
13. Gouveia DS, Rosenhaim R, de Maurera MAMA, Lima SJG, Paskocimas CA, Longo E, et al. Thermal study of $Co_xZn_{7-x}Sb_2O_{12}$ spinel obtained by Pechini method using different alcohols. J Therm Anal Calorim. 2004;75:453–60.
14. Gajbhiye NS, Prasad S. Thermal decomposition of hexahydrated nickel iron citrate. Thermochim Acta. 1996;285:325–36.
15. Wang L-Y, Wu G-Q, Evans DG. Synthesis and characterization of a layered double hydroxide containing an intercalated nickel(II) citrate complex. Mater Chem Phys. 2007;104:133–40.
16. Gajbhiye NS, Bhattacharya U, Darshane VS. Thermal decomposition of zinc–iron citrate precursor. Thermochim Acta. 1995; 264:219–30.
17. Dollimore D, Griffiths DL, Nicholson D. The thermal decomposition of oxalates. Part II. Thermogravimetric analysis of various oxalates in air and in nitrogen. J Chem Soc. 1963; 488:2617–23.
18. Lo Jacono M, Schiavello M, Cimino A. Structural, magnetic, and optical properties of nickel oxide supported on η- and γ-aluminas. J Phys Chem. 1971;75:1044–50.
19. Lenglet M, Hochu F, Dürr J, Tuilier MH. Investigation of the chemical bonding in $3d^8$ nickel (II) charge transfer insulators (NiO, oxidic spinels) from ligand-field spectroscopy, Ni 2p XPS and X-ray absorption spectroscopy. Solid State Commun. 1997; 104:793–8.
20. Llusar R, Casarrubios M, Barandiarán Z, Seijo L. Ab initio model potential calculations on the electronic spectrum of Ni^{2+}-doped MgO including correlation, spin-orbit and embedding effects. J Chem Phys. 1996;105:5321–30.
21. Lin B-Z, Li Z, Xu B-H, He L-W, Liu X-Z, Ding C. First Strandberg-type polyoxotungstate compound: synthesis and characterization of organic–inorganic hybrid $(H_2en)(Hen)_2[H_2P_2W_5O_{23}]\cdot 5.42H_2O$. J Mol Struct. 2006;825:87–92.
22. Redfern SAT. Hard-mode infrared study of the ferroelastic phase transition in $CuWO_4$–$ZnWO_4$ mixed crystals. Phys Rev B Condens Matter Mater Phys. 1993;48:5761–5.
23. Hanuza J, Macalik L, Maczka M, Lutz ETG, van der Maas JH. Vibrational characteristics of the double oxygen bridge in the $NaIn(WO_4)_2$ and $NaSc(WO_4)_2$ tungstates with wolframite structure. J Mol Struct. 1999;511:85–106.
24. Hanuza J, Maczka M, Hermanowicz K, Deren PJ, Strek W, Folcik L, et al. Spectroscopic properties and magnetic phase transitions in Scheelite $M^ICr(MoO_4)_2$ and Wolframite $M^ICr(WO_4)_2$ crystals, where M^I = Li, Na, K, and Cs. J Solid State Chem. 1999;148:468–78.
25. Hanuza J, Maczka M, Van der Mass JH. Vibrational properties of double tungstates of the $M^IM^{III}(WO_4)_2$ family (M^I = Li, Na, K; M^{III} = Bi, Cr). J Solid State Chem. 1995;117(1):177–88.
26. Orhan E, Anicete-Santos M, Maurera MAMA, Pontes FM, Souza AG, Andrès J, et al. Towards an insight on the photoluminescence of disordered $CaWO_4$ from a joint experimental and theoretical analysis. J Solid State Chem. 2005;178:1284–91.
27. Frost RL, Duong L, Weier M. Raman microscopy of selected tungstate minerals. Spectrochim Acta Part A. 2004;60:1853–9.
28. Nakamoto K, editor. Infrared and Raman spectra of inorganic and coordination compounds. New York: Wiley; 1980.
29. Nyquist RA, Kagel RO. Infrared spectra of inorganic compounds. London: Academic Press, Inc.; 1971.